

# Dielectric studies of freezing behavior in porous materials: Water and methanol in activated carbon fibres

M. Sliwinska-Bartkowiak,<sup>a</sup> G. Dudziak,<sup>a</sup> R. Sikorski,<sup>a</sup> R. Gras,<sup>a</sup> K. E. Gubbins<sup>b</sup> and R. Radhakrishnan<sup>b†</sup>

<sup>a</sup> Institute of Physics, Adam Mickiewicz University, Umultowska 85, 61-614 Poznan, Poland

<sup>b</sup> North Carolina State University, 113 Riddick Laboratories, Raleigh, NC 27695-7905, USA

Received 6th December 2000, Accepted 29th January 2001

First published as an Advance Article on the web 13th March 2001

We report both experimental measurements and molecular simulations of the melting and freezing behavior of two dipolar fluids, water and methanol, in activated carbon fibres. Differential scanning calorimetry (DSC) and dielectric relaxation spectroscopy (DS) were used to determine the melting point in these porous materials. The melting point was found to be very sensitive to the relative strength of the fluid–wall interaction compared to the fluid–fluid interaction. Monte Carlo simulations and the Landau free energy formalism were used to determine the shift in the melting point,  $T_m$ , for simple fluids in pores having weakly attractive and strongly attractive walls. The strength of the interaction of the fluid with the pore wall is shown to have a large effect on the shift in  $T_m$ , with  $T_m$  being reduced for weakly attracting walls and elevated for strongly attracting walls.

## 1. Introduction

Recently there has been growing interest in the study of fluid–solid transitions in porous materials. Important questions are the nature of the phase transition (first order *vs.* continuous), the direction of shift in the melting temperature  $T_m$ , nature and origin of hysteresis, dimensionality cross-over due to increasing confinement, structural changes of the condensed phases in the restricted pore geometries, effect on latent heats, *etc.* Improved understanding of confinement effects on freezing are essential in areas relating to lubrication, adhesion, fabrication of nanomaterials and nanotribology. In addition, these studies can provide insight into mechanisms involved in frost heaving and distribution of pollutants in soil. Freezing in porous media has also been widely employed in the characterization of porous materials using the method of thermoporometry. Some other possible applications are in the development of novel materials for energy storage, high-speed vehicles and aircraft braking systems.<sup>1,2</sup>

Experiments on melting that have used porous silica glass as the confinement medium have always resulted in a decrease in the melting temperature,  $T_m$ , as compared to the bulk. Melting of oxygen in sol–gel glasses was studied by Warnock *et al.*<sup>3</sup> by a sub-picosecond optical technique. In this method, birefringence in optical pump pulses caused by the rotational motion of the molecules in the liquid was used to measure the subsequent molecular orientational relaxation time. A change in the value of the relaxation time provided an indication of the freezing temperature. The melting temperature in the confined system was always depressed as compared to the bulk; the shift was larger for smaller pores, and as large as 10 K for the smallest (20 nm) pore. Unruh and co-workers<sup>4</sup> examined the melting behavior of indium metal in porous silica glasses by differential scanning calorimetry (DSC) measurements, and reported a large depression in melting point due to confine-

ment. In view of the large body of experimental evidence for a decrease in the melting temperature due to confinement (ref. 5 and references therein), it is tempting to assume that a decrease always occurs. However, a classical thermodynamic argument based on simple capillary theory determines the melting temperature as the point at which the chemical potential of the solid core inside the pore equals that of the surrounding fluid (for example, see ref. 5),

$$\frac{\Delta T_m}{T_{mb}} = -2 \frac{(\gamma_{ws} - \gamma_{wl})v}{H\lambda_{mb}} \quad (1)$$

where  $T_{mb}$  is the bulk melting temperature,  $\gamma_{ws}$  and  $\gamma_{wl}$  are the corresponding wall–solid and wall–fluid surface tensions,  $v$  is the molar volume of the liquid,  $\lambda_{mb}$  is the latent heat of melting in the bulk and  $H$  is the pore width. Eqn. (1) is sometimes referred to as the Gibbs–Thomson equation, and predicts that the sign of  $\Delta T_m = T_m - T_{mb}$  depends on whether  $\gamma_w$  is greater or less than  $\gamma_{wl}$ . In a molecular simulation study of the effect of confinement on freezing of simple fluids in slit pores by Miyahara and Gubbins,<sup>6</sup> it was shown that  $T_m$  was strongly affected by the strength of the attractive forces between the fluid molecules and the pore walls. For repulsive or weakly attractive potentials, the shift in the freezing temperature  $\Delta T_m$  was negative. For strongly attracting walls such as carbons, an *increase* in  $T_m$  was observed. Thus, Miyahara and Gubbins explained the disparate experimental trends on the direction of the shift in the freezing temperature and provided the connection to the Gibbs–Thomson equation. The predictions of Miyahara and Gubbins were confirmed by free energy studies that provided the thermodynamic freezing temperature in confined systems; these studies established that the freezing transition remained first order despite the varied dimensionality.<sup>7,8</sup>

The first experimental evidence of an elevation in freezing temperature for confined systems was reported by Klein and Kumacheva.<sup>9</sup> These authors studied the properties of cyclohexane films confined between parallel mica surfaces (slit-shaped geometry). They observed a sudden change in the surface force, accompanied by a change to solid-like behavior

† Current address: Massachusetts Institute of Technology, Chemical Engineering Department, 77 Mass. Ave., Cambridge, MA 02139, USA.

of the film, at a particular separation of the mica surfaces. They interpreted this change as a freezing transition. The transition temperature was about 17 K *above* the melting temperature for bulk cyclohexane, for a pore width of 4.0 nm. Similar phenomena have been observed for linear alkanes confined between mica surfaces.<sup>10,11</sup> More recently, Castro *et al.*<sup>12</sup> studied freezing of methane and other liquid alkanes on a graphite substrate by incoherent elastic neutron scattering. They found that the layer nearest to the graphite substrate melts at a temperature 10% higher than the bulk melting point of methane. The elevation in the freezing temperature in confined systems remains controversial, as there have been contradicting reports on the nature of the shift in the freezing temperature of cyclohexane between parallel mica surfaces in a surface force apparatus.<sup>13</sup>

In this article, we report a study of the effect of the strength of the pore wall interaction on the freezing/melting behavior of confined fluids. Results are presented for water and methanol in activated carbon fibres; while both fluids have relatively strong fluid–fluid interactions, the fluid–wall interaction is strong for methanol and rather weak in the case of water. The DSC and dielectric spectroscopy experiments were performed at Adama Mickiewicza University, Poznan, Poland, and the molecular simulations were performed at North Carolina State University, USA.

## 2. Methods

### Molecular simulation

We performed grand canonical Monte Carlo (GCMC) simulations of Lennard-Jones fluids adsorbed in regular slit-shaped pores of pore width  $H$  and varying fluid–wall strengths. Here  $H$  is the distance separating the planes through the centres of the surface-layer atoms on opposing pore walls. The interaction between the adsorbed fluid molecules is modeled using the Lennard-Jones (12,6) potential. The fluid–wall interaction is modeled using a “10-4-3” Steele potential,<sup>14</sup>

$$\phi_{\text{fw}}(z) = 2\pi\rho_w \varepsilon_{\text{fw}} \sigma_{\text{fw}}^2 \Delta \left[ \frac{2}{5} \left( \frac{\sigma_{\text{fw}}}{z} \right)^{10} - \left( \frac{\sigma_{\text{fw}}}{z} \right)^4 - \left( \frac{\sigma_{\text{fw}}^4}{3\Delta(z + 0.61\Delta)^3} \right) \right] \quad (2)$$

Here,  $\sigma$  and  $\varepsilon$  are the size and energy parameters in the LJ potential, the subscripts f and w denote fluid and wall respectively,  $\rho_w$  is the number density of the atoms in the wall,  $\Delta$  is the distance between two successive lattice planes in graphite, and  $z$  is the coordinate perpendicular to the pore walls. The fluid–wall interaction energy parameters corresponding to a graphite pore were taken from ref. 14. For a given pore width  $H$ , the total potential energy from both walls is given by,

$$\phi_{\text{pore}}(z) = \phi_{\text{fw}}(z) + \phi_{\text{fw}}(H - z) \quad (3)$$

The strength of the fluid–wall relative to the fluid–fluid attraction is determined by the parameter  $\alpha = \rho_w \varepsilon_{\text{fw}} \sigma_{\text{fw}}^2 \Delta / \varepsilon_{\text{ff}}$ . For example, in the case of methane,  $\alpha = 0$  corresponds to a purely repulsive or hard wall,  $\alpha = 0.76$  corresponds to a weakly attractive wall and  $\alpha = 2.0$  corresponds to a strongly attractive graphite wall. Our objective is to calculate the freezing temperatures in the confined phase as a function of the relative strengths of the fluid–wall and the fluid–fluid interaction,  $\alpha$ . Following Radhakrishnan *et al.*,<sup>15</sup> we can use the theory of corresponding states to show that for small adsorbate molecules the reduced freezing temperature of a LJ fluid in our model slit pore depends only on the values of  $\alpha$  and  $H^* = H/\sigma_{\text{ff}}$ , to a good approximation. We can use this powerful result to compare the simulation results with our experimental results. For the real systems we have studied (see Section 4), *viz.*, water and methanol in activated carbon fiber (ACF), we

calculate the value of  $\alpha$  using parameters of the Lennard-Jones potential that reproduce thermophysical data (see ref. 15).

The simulation runs were performed in the grand canonical ensemble, fixing the chemical potential  $\mu$ , the volume  $V$  of the pore and the temperature  $T$ . A pore width of  $H = 3\sigma_{\text{ff}}$  was chosen to enable comparison with our experimental results. The system consisted of 600–12000 adsorbed molecules, depending on system size. For the case of attractive pore–wall interaction, the adsorbed molecules formed distinct layers parallel to the plane of the pore walls. A rectilinear simulation cell of dimensions  $L \times L$  (where  $L$  was varied between  $10\sigma_{\text{ff}}$  and  $60\sigma_{\text{ff}}$ ) in the plane parallel to the pore walls was used. The simulation was set up such that insertion, deletion and displacement moves were attempted with equal probability, and the displacement step was adjusted to have a 50% probability of acceptance. Thermodynamic properties were averaged over  $100\text{--}2000 \times 10^6$  individual Monte Carlo steps. The length of the simulation was adjusted such that a minimum of fifty times the average number of particles in the system would be inserted and deleted during a single simulation run.

### Free energy method

The method relies on the calculation of the Landau free energy as a function of an effective bond orientational order parameter  $\Phi$ , using GCMC simulations.<sup>8</sup> The Landau free energy  $A$  is defined by,

$$A[\Phi] = -k_{\text{B}}T \ln(P[\Phi]) + \text{constant} \quad (4)$$

where  $P[\Phi]$  is the probability of observing the system having an order parameter value between  $\Phi$  and  $\Phi + \delta\Phi$ . The probability distribution function  $P[\Phi]$  is calculated in a GCMC simulation as a histogram, with the help of umbrella sampling. The grand free energy  $\Omega$  is then related to the Landau free energy by

$$\exp(-\beta\Omega) = \int d\Phi \exp(-\beta A[\Phi]) \quad (5)$$

The grand free energy at a particular temperature can be calculated by numerically integrating eqn. (5) over the order parameter space. We use a two-dimensional order parameter to characterize the order in each of the molecular layers.

$$\Phi_j = \left| \frac{1}{N_{\text{b}}} \sum_{k=1}^{N_{\text{b}}} \exp(i6\theta_k) \right| = |\langle \exp(i6\theta_k) \rangle_j| \quad (6)$$

$\Phi_j$  measures the hexagonal bond order within each layer  $j$ . Each nearest neighbor bond has a particular orientation in the plane of the given layer, and is described by the polar coordinate  $\theta$ . The index  $k$  runs over the total number of nearest neighbor bonds,  $N_{\text{b}}$  in layer  $j$ . The overall order parameter  $\Phi$  is an average of the hexagonal order in all the layers. We expect  $\Phi_j = 0$  when layer  $j$  has the structure of a two-dimensional liquid,  $\Phi_j = 1$  in the crystal phase and  $0 < \Phi_j < 1$  in an orientationally ordered layer.

### Differential scanning calorimetry

Two different fluids, *viz.*, water and methanol were chosen for study. Activated carbon fibres were chosen as the confinement media. Perkin-Elmer and Dupont thermal analyzers were used to determine the melting temperatures and latent heats of fusion, by measuring the heat released in the melting of the bulk fluid and confined fluid. Temperature scanning rates of  $0.5\text{--}2 \text{ K min}^{-1}$  were used in the experiments. The melting temperatures were determined from the position of the peaks of the heat flow signals and the latent heats were determined based on the scaled area under these signals. The melting temperatures were reproducible to within  $0.5^\circ\text{C}$  for larger pores ( $\geq 25 \text{ nm}$ ); uncertainties were larger for the smaller pores. The latent heats were reproducible to within an accuracy of 5%.

**Table 1** Melting temperatures in the confined phase obtained from simulation

System	$\alpha^a$	$T_{m, \text{pore}}/T_{m, \text{bulk}}$	$T_{h, \text{pore}}/T_{m, \text{bulk}}$
Water/ACF	0.45	0.92	None
	0.70	0.98	None
Methanol/ACF	1.35	1.15	1.28

<sup>a</sup> From ref. 15.

### Dielectric method

Freezing of a dipolar liquid is accompanied by a rapid decrease in its electric permittivity.<sup>16–18</sup> After the phase transition to the solid state, dipole rotation ceases and the electric permittivity is almost equal to  $n^2$ , as it arises from deformation polarization only; here  $n$  is the refractive index of the solid. Therefore dielectric spectroscopy is suitable for investigation of the phenomena of melting and freezing of dipolar liquids, because of significant changes of the system's capacity at the phase transition. Investigation of the dynamics of a confined liquid is possible from the frequency dependences of dielectric properties for such systems. Analysis of the frequency dependence of dielectric data allows a determination of the phase transition temperature of the adsorbed substance and of characteristic relaxation frequencies related to molecular motion in particular phases.<sup>19,20</sup>

**Dielectric relaxation spectroscopy.** The dielectric relaxation method was applied to study the process of freezing of a sample of two confined dipolar liquids: water and methanol on activated carbon fibres (ACF) of type P20, having a mean pore size  $H = 1.8 \text{ nm}$ .<sup>21</sup> The complex electric permittivity,  $\kappa = \kappa' + i\kappa''$ , where  $\kappa' = C/C_0$  is the real, and  $\kappa'' = \tan(\delta)/\kappa'$  is the complex part of the permittivity, was measured in the frequency interval 300 Hz–1 MHz at different temperatures by a Solartron 1200 impedance gain analyser, using a parallel plate capacitor made of stainless steel. In order to reduce the high conductivity of the sample, which was placed between the capacitor plates as a suspension of water- or methanol-filled ACF particles in pure liquids, the electrodes were covered with a thin layer of Teflon. From the directly measured capacitance  $C$  and the tangent loss  $\tan(\delta)$ , the values of  $\kappa'$  and  $\kappa''$  were calculated for the known sample geometry.<sup>19</sup> The temperature was controlled to an accuracy of 0.1 K using a platinum resistor Pt(100) as a sensor and a K30 Modinegen external cryostat coupled with a N-180 ultra-cryostat.

The water samples were distilled and demineralised on ionites using a Multipore apparatus. The conductivity of the purified water was on the order of  $10^{-6} \Omega^{-1} \text{ m}^{-1}$ . The methanol samples were dried over sodium, fractionally distilled and kept over molecular sieves C3. The conductivity was less than  $10^{-8} \Omega^{-1} \text{ m}^{-1}$ . The pore materials to be used in the experiment were heated to about 600 K, and kept under vacuum ( $\sim 10^{-3}$  Torr) for 6 days prior to the introduction of the fluid.

For an isolated dipole rotating under an oscillating field in a viscous medium, the Debye dispersion relation is derived in terms of classical mechanics:

$$\kappa^* = \kappa'_\infty + \frac{\kappa'_s + \kappa'_\infty}{1 + (i\omega\tau)}, \quad (7)$$

where  $\omega$  is the frequency of the potential applied, and  $\tau$  is the orientational relaxation time of a dipolar molecule. The subscript "s" refers to the static permittivity, *i.e.* the permittivity in the low frequency limit, when the dipoles have enough time to be in phase with the applied field. The subscript  $\infty$  refers to the high frequency limit of the permittivity, and is a measure of the induced component of the permittivity. The dielectric relaxation time was calculated by fitting the dispersion spec-

trum of the complex permittivity near resonance to the Debye model of orientational relaxation.

### 3. Simulation results

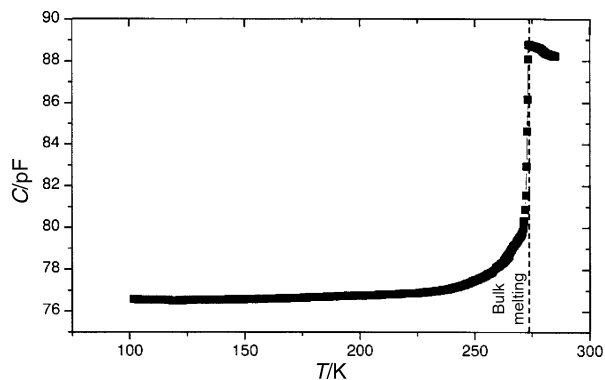
We performed molecular simulations and Landau free energy calculations for a LJ fluid confined in a slit-shaped pore of width  $H = 3\sigma_{\text{eff}}$ , of varying fluid–wall interaction strengths. The value of  $\alpha$  (see Section 2) was varied from  $\alpha = 0.45$  (corresponding to water confined in ACF) to  $\alpha = 1.5$  (corresponding to methanol confined in ACF), to model a range of pore wall potentials, ranging from weakly attractive to strongly attractive.

The Landau free energy calculations showed that for systems with a value of  $\alpha < 0.73$ , *i.e.*, for a fluid confined in a weakly attractive pore, the freezing temperature in the confined phase is less than that of the bulk phase. The opposite is true for systems with  $\alpha > 0.73$ , *i.e.*, for a fluid confined in a strongly attractive pore. The freezing temperatures of the confined phase expressed as  $T_{m, \text{pore}}/T_{m, \text{bulk}}$  for different values of  $\alpha$  are shown in Table 1. For the case of strongly attractive pores ( $\alpha > 0.73$ ), there was an additional phase transition from a liquid-like phase to an orientationally ordered hexatic phase at higher temperature,  $T_{h, \text{pore}}$ .

### 4. Experimental results

#### Water

The capacitance  $C$  and loss tangent  $\tan(\delta)$  were measured as a function of frequency and temperature for bulk water and for water adsorbed in ACF, from which the dielectric permittivity  $\kappa'(T, \omega)$  and  $\kappa''(T, \omega)$  were calculated. Results of the measurements of  $C$  for bulk water as a function of  $T$  and at a frequency of 0.6 MHz, are shown in Fig. 1. There is a sharp increase in  $C$  at  $T = 273 \text{ K}$ , the melting point of the pure substance, due to the contribution to the orientational polarisation<sup>16,17</sup> in the liquid state from the permanent dipoles. In the frequency interval studied we could only detect the low-frequency relaxation of water. Analysis of the Cole–Cole representation of the complex permittivity for solid water has shown that the relaxation observed should be approximated by a symmetric distribution of relaxation times described formally by the Cole–Cole equation (1). Examples of the experimental results and the fitted curves are given in Fig. 2(a) and (b) for the bulk solid phase at 137 K. From the plot of  $\kappa'$  and  $\kappa''$  vs.  $\log \omega$  (Fig. 2), the relaxation time can be calculated as the inverse of the frequency corresponding to a saddle point of the  $\kappa'$  plot or a maximum of the  $\kappa''$  plot. An alternative graphical representation of the Debye dispersion equation is the Cole–Cole diagram in the complex  $\kappa^*$  plane (Fig. 2(b)). Each relaxation mechanism is reflected as a semicircle in the Cole–Cole diagram. From the plot of  $\kappa''$  vs.  $\kappa'$ , the value of  $\tau$  is

**Fig. 1** Capacitance  $C$  vs. temperature  $T$  for bulk water,  $\omega = 0.6$  MHz.

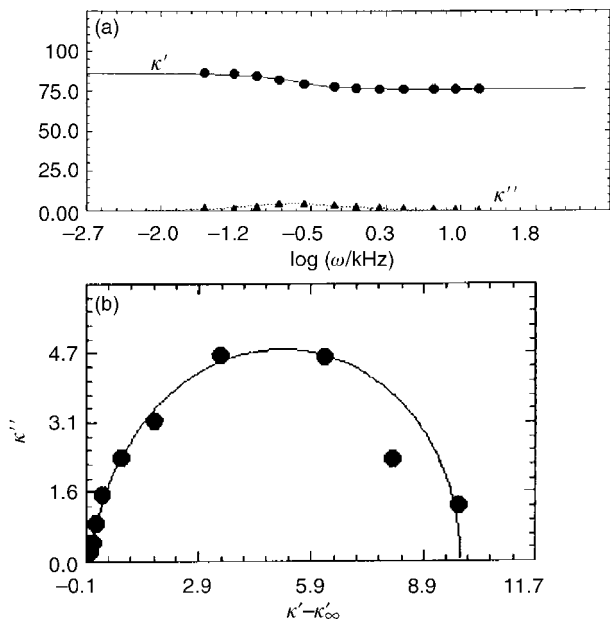


**Fig. 2** (a) Spectrum plot for solid bulk water at 137 K (the solid and the dashed curves are fits to the real and imaginary parts of  $\kappa$ ). (b) Representation of the spectrum plots in the form of a Cole–Cole diagram for water at 137 K.

given as the inverse of the frequency at which  $\kappa''$  goes through a maximum.

Fig. 3 presents the variation of the relaxation time with temperature for bulk water obtained from fitting eqn. (7) to the dispersion spectrum. In the solid phase (below 273 K), our measurements showed the ordinary ice to have a single relaxation time of the order of  $10^{-5}$ – $10^{-3}$  s in the temperature range from 273 to 200 K respectively, which is consistent with other results.<sup>16</sup> The liquid branch above 273 K has rotational relaxation times of the order of  $10^{-12}$  s.<sup>16,17</sup> This branch lies beyond the possibilities of our analyser. In the presence of dipolar constituents, one or more absorption regions are present, not all of them necessarily associated with the dipolar dispersion. At the lowest frequencies (especially about 1 KHz), a large  $\kappa''$  value arises from the conductivity of the medium, and interfacial (Maxwell–Wagner) polarisation is found if the system is not in a single homogeneous phase. For water, a homogeneous medium whose conductivity is of the order of  $10^{-6} \Omega^{-1} \text{ m}^{-1}$ , the absorption region observed for the frequencies 1–10 KHz is related to the conductivity of the medium. The Joule heat arising from the conductivity contributes to a loss factor  $\kappa''$  (conductance) so that the value at low frequency is:  $\kappa''_{\text{total}} = \kappa''_{\text{dielectric}} + \kappa''_{\text{conductance}}$  and the system reveals the energy loss in processes other than dielectric relaxation. In Fig. 3 the branch above 273 K, corresponding to the

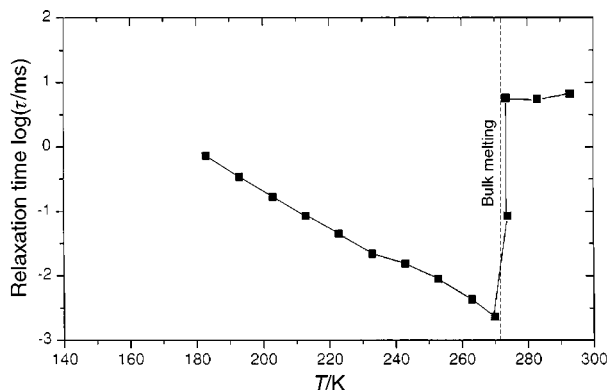


**Fig. 3** Dielectric relaxation time,  $\tau$ , vs.  $T$  for bulk water.

relaxation times of the order of  $10^{-3}$  to  $10^{-2}$  s, characterises the process of absorption related to the conductivity of the medium. This branch is characteristic of the liquid phase and is a good indicator of the appearance of the phase.

The behavior of  $C$  vs.  $T$  for water in ACF at a frequency of 0.6 MHz is shown in Fig. 4. The sample was introduced between the capacitor plates as a suspension of ACF in pure water. As follows from Fig. 2, the value of  $C$  undergoes two sudden changes—at 273 K related to the bulk solid–liquid transition and at 235 K. The character of the change observed at 235 K is very similar to that corresponding to the melting of a dipolar liquid placed in porous glass,<sup>19,20</sup> and the scanning calorimetry results for this system have indicated a phase transition at 235 K.<sup>20</sup> Therefore, it can be assumed that this is the temperature of melting of ice confined in ACF. If we assume that ice in ACF melts at 235 K, below this temperature the system should contain only ice; in the range 235–273 K water should be present in the bulk crystal phase and also as liquid in the pores, and above 273 K as bulk liquid and liquid in the pores.

Fig. 5(a) and 6(a) present the spectrum plot ( $\kappa'$ ,  $\kappa''$  vs.  $\omega$ ) for water confined in ACF at two different temperatures. The spectrum in Fig. 5(a), for 180 K, corresponds to one relaxation mechanism characterised by a relaxation time of the order of  $10^{-4}$  s, which is typical of ice at this temperature. The spec-

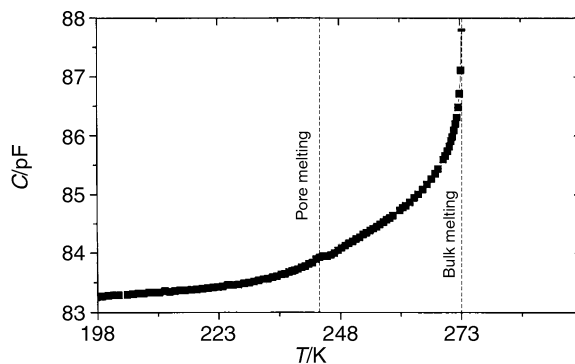


**Fig. 4**  $C$  vs.  $T$  for water in ACF at  $\omega = 0.6$  MHz.

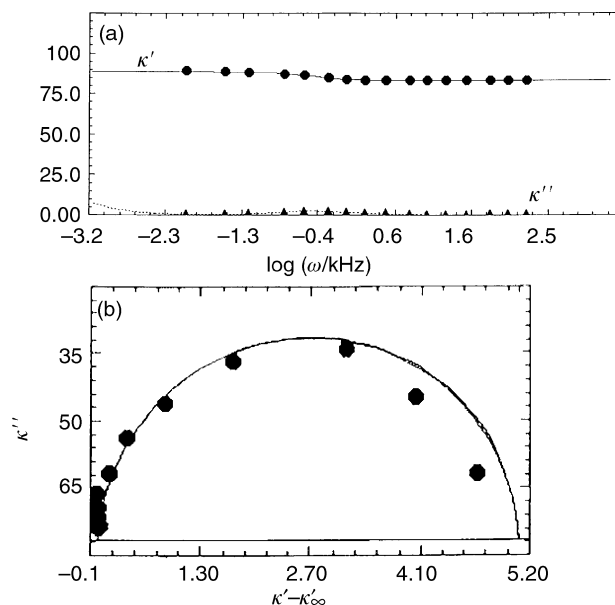


**Fig. 5** (a) Spectrum plot for water at 180 K (the solid and the dashed curves are fits to the real and imaginary parts of  $\kappa$ ). (b) Representation of the spectrum plots in the form of a Cole–Cole diagram for water in ACF at 180 K.

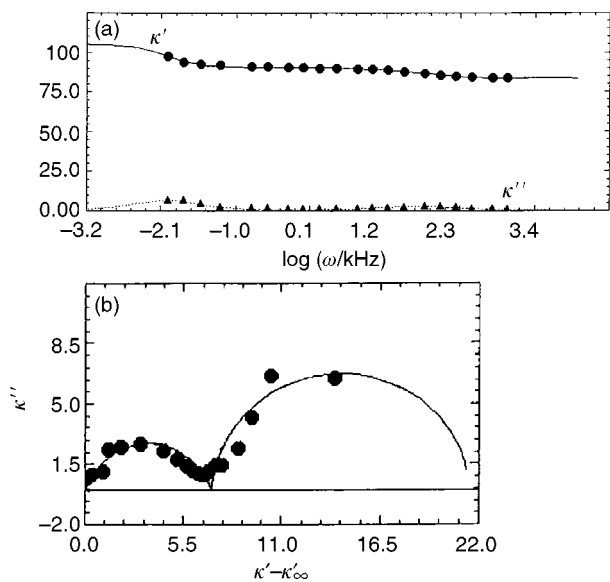


**Fig. 6** (a) Spectrum plot for water in ACF at 243 K (the solid and the dashed curves are fits to the real and imaginary parts of  $\kappa$ ). (b) Representation of the spectrum plots in the form of a Cole-Cole diagram for water in ACF at 243 K.

trum in Fig. 6(a), for 243 K, represents two relaxation mechanisms, as indicated by the two inflection points in  $\kappa'$ , characterised by relaxation times of the order of  $10^{-3}$  and  $10^{-5}$  s. The corresponding Cole-Cole diagrams are shown in Fig. 5(b) and 6(b). Each relaxation mechanism corresponds to a semi-circle in the Cole-Cole diagram. Therefore, Fig. 5 confirms the presence of one relaxation mechanism at the lower temperature (180 K), and Fig. 6 at 243 K indicates two relaxation mechanisms.

The behavior of the relaxation times as a function of temperature for water in ACF is depicted in Fig. 7. For temperatures higher than 235 K (melting point inside the pores) there are two different kinds of relaxation. The larger component of the relaxation time of the order of  $10 \times 10^{-3}$  s is strongly dependent on temperature. It could be related to the conductivity of water in pores, and testifies to the presence of the liquid phase in the system. The shorter component of the relaxation time is of the order of  $10^{-6}$  s and is characteristic of the solid state of bulk water in this temperature range. The longer component is also observed above the bulk melting temperature, where the additional contribution of the Maxwell-Wagner interfacial polarisation takes place. The Maxwell-Wagner effect disappears below the bulk melting point because the ACF particles are arrested in the crystalline matrix of bulk water, thereby preventing interfacial dispersion. Below the pore melting point, in the range 235–160 K, a

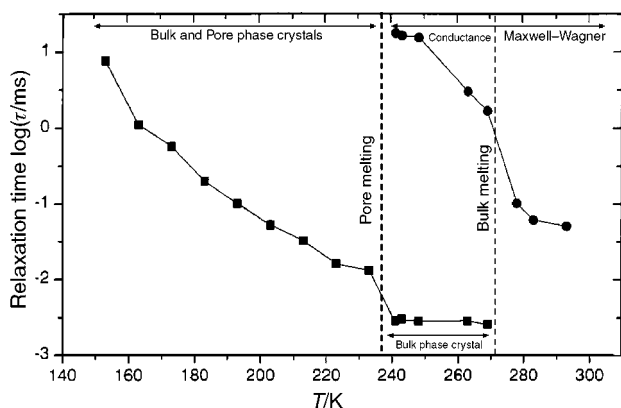


**Fig. 7**  $\tau$  vs.  $T$  for water in ACF.

branch of shorter relaxation times is observed, characteristic of Debye-type dispersion in ice; the crystal phase of water occurs both in the pores and in bulk water. The results obtained show that the ice melting point in the ACF pores is 235 K, which is 38 K lower than in the bulk. They also suggest that while liquid-like and crystalline regions can exist in the pore space, there is no evidence of additional amorphous phases, or glassy or contact-layer phases.<sup>15,19,20</sup> The relaxation times determined indicate the presence of only solid or liquid micro-phases in the pores.

### Methanol

The process of melting of methanol in the ACF pores is more complex than for water. Methanol has two crystalline phases.<sup>22</sup> The  $\alpha$  phase, with orthorhombic  $P2_12_12_1$  structure and 4 molecules in the elementary cell, is stable below 156 K; the  $\beta$  phase, also orthorhombic with 4 molecules in the elementary cell but of symmetry  $Cmc2_1$ , exists between 159 K and the melting point, 175.4 K. The transition from the  $\alpha$  to the  $\beta$  phase occurs in two steps: a first-order transition takes place at 156 K, and a second-order one at 160 K. The structure between the two temperatures has not been characterised yet. In Fig. 8 we present the dependence of  $C(T)$  for bulk methanol. An abrupt increase at 156 K corresponds to the first order transition between the phases  $\alpha$  and  $\beta$ ; the increase in  $C$  at 161 K is related to the second-order transition from the  $\alpha$  to the  $\beta$  phase; and the large increase in  $C$  at 175 K corresponds to the phase transition from the  $\beta$  phase to the liquid phase.

In Fig. 9 we present  $C$  vs.  $T$  for methanol confined in ACF. We observe three abrupt increases in  $C$ , at 157, 218 and 256 K. The increase at 157 K corresponds to the transition from the  $\alpha$  to the  $\beta$  phase in the bulk material (and possibly in the pores). Comparison of the experimental results with those

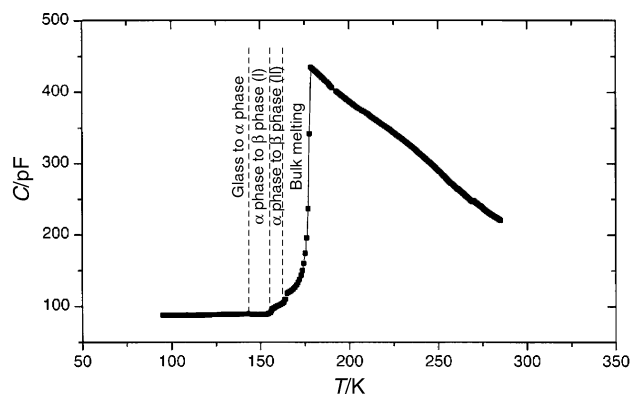


**Fig. 8**  $C$  vs.  $T$  for methanol at frequency 0.6 MHz.

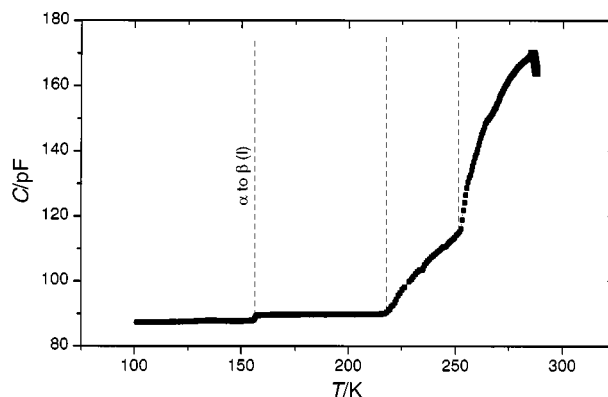


**Fig. 9**  $C$  vs.  $T$  for methanol in ACF at frequency 0.6 MHz.

**Table 2** Melting temperatures in the confined phase obtained from experiment

System	$\alpha^a$	$T_{m, \text{pore}}/T_{m, \text{bulk}}$	$T_{h, \text{pore}}/T_{m, \text{bulk}}$
Water/ACF	0.45	0.87	None
Methanol/ACF	1.35	1.25	1.42

<sup>a</sup> From ref. 15.

from molecular simulations for our simple model of the methanol/ACF system suggest that the abrupt change at 218 K may be due to a crystal–hexatic transition, while that at 256 K may be due to a hexatic to liquid transition. A summary of the observed transition temperatures in the pore, relative to the bulk values and assuming that this interpretation is correct, is shown in Table 2. These values can be compared with those from simulation given in Table 1. The simulation and experimental values are in qualitative agreement. Further experimental studies are needed to clarify the nature of these transitions. We plan to carry out X-ray scattering studies, and also an analysis of the dielectric relaxation times for this system, in order to characterize these phases.

We note that the two transitions associated with melting in the ACF pores (at 218 and 256 K) occur at temperatures much higher than for the bulk material ( $T_m = 175.4$  K) as predicted by the simulations.

## 5. Discussion

We have studied freezing/melting phenomena in confined phases in ACF as a function of the relative strengths of the fluid–wall and the fluid–fluid interaction,  $\alpha$ . There is qualitative agreement between the results of our simulations and experiment (see Tables 1 and 2). We note that we are able to adjust the value of  $\alpha$  by varying the dipole moment of the fluid molecule. The fluid–fluid interaction is strongly dependent on the dispersive as well as the dipolar components. However, owing to the small polarizability of the pore walls of ACF, the fluid–wall interaction depends primarily on the dispersive component of the fluid molecules. Therefore, when confined in ACF, the fluid molecules with greater dipole moment experience a smaller  $\alpha$  value compared to those with smaller dipole moment. This is the reason why there is a lowering of the melting temperature for water confined in ACF ( $\alpha = 0.45$ ), while methanol confined in ACF shows an elevation in the freezing temperature ( $\alpha = 1.35$ ).

In the future, we plan to develop global phase diagrams from simulation and experiment, to summarize the diverse freezing behavior of different fluids in different porous materials; this work is in progress and will be published elsewhere.<sup>23</sup> Efforts are also underway to use more realistic fluid potentials and pore models<sup>24,25</sup> in the simulations. The pro-

posed models include networking and polydispersity effects and reproduce the structures of the real porous material quite closely.

## Acknowledgements

This work was supported by grants from the National Science Foundation (Grant No. CTS-9896195), and by a grant from the U.S.-Poland Maria Sklodowska-Curie Joint fund (grant no. MEN/DOE-97-314). Supercomputer time was provided under a NSF/NRAC grant (MCA93S011).

## References

- 1 *Proceedings of COPS-V, 5th International Symposium on the Characterization of Porous Solids*, Elsevier, Amsterdam, 1999.
- 2 *Proceedings of the 24th Biennial Conference on Carbon*, American Carbon Society, Charleston, SC, 1999.
- 3 J. Warnock, D. D. Awschalom and M. W. Shafer, *Phys. Rev. Lett.*, 1986, **57**(14), 1753.
- 4 K. M. Unruh, T. E. Huber and C. A. Huber, *Phys. Rev. Sect. B*, 1993, **48**(12), 9021.
- 5 M. Sliwinska-Bartkowiak, J. Gras, R. Sikorski, R. Radhakrishnan, L. D. Gelb and K. E. Gubbins, *Langmuir*, 1999, **15**, 6060.
- 6 M. Miyahara and K. E. Gubbins, *J. Chem. Phys.*, 1997, **106**(7), 2865.
- 7 H. Dominguez, M. P. Allen and R. Evans, *Mol. Phys.*, 1999, **96**, 209.
- 8 R. Radhakrishnan and K. E. Gubbins, *Mol. Phys.*, 1999, **96**, 1249.
- 9 J. Klein and K. Kumacheva, *Science*, 1995, **269**, 816.
- 10 H. W. Hu, G. A. Carson and S. Granick, *Phys. Rev. Lett.*, 1991, **66**, 2758.
- 11 S. Granick, *Science*, 1991, **253**, 1374.
- 12 M. A. Castro, S. M. Clarke, A. Inaba and R. K. Thomas, *J. Phys. Chem. B*, 1998, **101**, 10528.
- 13 H. K. Christenson, *Colloids Surf. A*, 1997, **123**, 355.
- 14 W. A. Steele, *Surf. Sci.*, 1973, **36**, 317.
- 15 R. Radhakrishnan, K. E. Gubbins and M. Sliwinska-Bartkowiak, *J. Chem. Phys.*, 2000, **112**(24), 11048.
- 16 N. Hill, W. E. Vaughan, A. H. Price and M. Davies, in *Dielectric Properties and Molecular Behaviour*, ed. T. M. Sugden, Van Nostrand Reinhold, New York, 1970.
- 17 A. U. Ahadov, *Dielektricheskoje Svoistva Zhidkih Zhidkosti*, Izdatelstvo Standartov, Moskva, 1972.
- 18 B. Szurkowski, T. Hilczer and M. Sliwinska-Bartkowiak, *Ber. Bunsen-Ges. Phys. Chem.*, 1993, **97**(5), 731.
- 19 M. Sliwinska-Bartkowiak, J. Gras, R. Sikorski, R. Radhakrishnan, L. Gelb and K. E. Gubbins, *Langmuir*, 1999, **15**(18), 6060.
- 20 M. Sliwinska-Bartkowiak, G. Dudziak, R. Sikorski, R. Gras, R. Radhakrishnan and K. G. Gubbins, *J. Chem. Phys.*, 2001, **114**, 950.
- 21 R. Radhakrishnan, K. E. Gubbins, A. Watanabe and K. Kaneko, *J. Chem. Phys.*, 1999, **111**, 9058.
- 22 B. H. Torrie, S.-X. Weng and B. M. Powell, *Mol. Phys.*, 1989, **67**(3), 575.
- 23 R. Radhakrishnan, K. E. Gubbins and M. Sliwinska-Bartkowiak, in preparation.
- 24 L. D. Gelb and K. E. Gubbins, *Langmuir*, 1998, **14**, 2097.
- 25 K. T. Thomson and K. E. Gubbins, *Langmuir*, 2000, **16**, 5761.